

## Gas sparged gel layer controlled cross flow ultrafiltration: A model for stratified flow regime and its validity

Vivek Khetan, Ashish Srivastava and Sirshendu De\*

Department of Chemical Engineering; Indian Institute of Technology, Kharagpur,  
Kharagpur – 721302, India

(Received October 14, 2011, Revised April 10, 2012, Accepted April 28, 2012)

**Abstract.** Gas sparging is one of the techniques used to control the concentration polarization during ultrafiltration. In this work, the effects of gas sparging in stratified flow regime were investigated during gel layer controlling cross flow ultrafiltration in a rectangular channel. Synthetic solution of pectin was used as the gel forming solute. The liquid and gas flow rates were selected such that a stratified flow regime was prevalent in the channel. A mass transfer model was developed for this system to quantify the effects of gas flow rates on mass transfer coefficient (Sherwood number). The results were compared with the case of no gas sparging. Gas sparging led to an increase of mass transfer coefficient by about 23% in this case. The limitation of the developed model was also evaluated and it was observed that beyond a gas flow rate of 20 l/h, the model was unable to explain the experimental observation, i.e., the decrease in permeate flux with flow rate.

**Keywords:** air sparging; stratified flow; gel layer; mass transfer coefficient; permeate flux

---

### 1. Introduction

Ultrafiltration is a pressure driven membrane separation process, and is used to concentrate, recover and remove macromolecules from aqueous solution (Rautenbach and Albrecht 1986). The commercial applications of ultrafiltration are antibody recovery in pharmaceutical industries (Rosenberg *et al.* 2009), latex or polymer concentration (Llanos *et al.* 2009), protein filtration in dairy industries (Mourouzidis-Mourouzis *et al.* 2008), water and wastewater treatment (Wu *et al.* 2006), etc.

Concentration polarization and membrane fouling are inherent limitations of ultrafiltration that leads to decline in throughput of the process (Porter 2005). Thus, techniques to reduce concentration polarization and membrane fouling are active area of research. The general approaches to reduce concentration polarization are categorized in chemical, hydrodynamic and physical methods. Chemical methods include use of conducting polymers (Zhao *et al.* 1993), heterogeneous chemical modification (Steuck and Reading 1986), adsorption of hydrophilic polymers, surface modification by ionic and non-ionic surfactants (Fane *et al.* 1985), irradiation method (Nystrom and Javinen 1991), low temperature plasma activation (Kramer *et al.* 1989) etc. Hydrodynamic methods involve use of turbulent promoters (Thomas 1973, DaCosta *et al.* 1993, Mackley and Sherman 1993), introduction of secondary flow (Chung *et al.* 1993) and pulsatile flow (Belfort *et al.* 1993, Finnigan and Howell 1990). In physical method, applications of external fields, like, ultrasonic (Najarian and Bellhouse 1996) and electric

---

\* Corresponding author, Professor, E-mail: [sde@che.iitkgp.ernet.in](mailto:sde@che.iitkgp.ernet.in)

field (Hermann 1982, Sarkar and De 2011) have been explored to reduce fouling. Gas sparging for flux enhancement during membrane processes belongs to the category of alteration of hydrodynamic conditions in the flow channel.

Plenty of literature regarding flux enhancement by gas sparging appeared in the decade of 1990. Imasaka *et al.* reported methane gas generated in a fermentor enhanced the permeate flux significantly in a ceramic module (Imasaka *et al.* 1989, Imasaka *et al.* 1993). Use of air slug increased the permeate flux during cross flow filtration (Lee *et al.* 1993, Mercier *et al.* 1997, Mercier *et al.* 2000). Effects of mounting angles of membrane module on permeate flux enhancement by gas slugs were also studied (Cheng *et al.* 1999, Cheng 2002). 7 to 50% flux enhancement for various single proteins and improvement of fractionation of proteins in a mixture were reported during gas sparged ultrafiltration (Bellara *et al.* 1997, Li *et al.* 1997, Li *et al.* 1998). Enhancement of membrane permeability by gas sparging upto 115% in submerged hollow fibre ultrafiltration is reported (Ghosh 2006). Cui and co-workers investigated the angle of mounting of modules, effects of various modules for gas sparged cross flow ultrafiltration of dye, Dextran and BSA molecules (Cui and Wright 1994, Cui and Wright 1996, Cabassud *et al.* 1997). An excellent review on selection and performance of gas sparged ultrafiltration systems and various applications is available (Cui *et al.* 2003). 125% increase of flux during ultrafiltration of PVP was obtained in a tubular module (Abdel-Ghani 2000). About 140% flux enhancement during Microfiltration of Oil-Water emulsion was reported by Ducom *et al.* (2002).

Significant amount of works are available to model the gas-sparged ultrafiltration system. Hydrodynamic models and their positive impact on mass transfer boundary layer are quite popular (Li *et al.* 1997, Cui and Wright 1994, Cui and Wright 1997, Ghosh and Cui 1999). Delgado *et al.* (2004) proposed a model of particle deposition in hollow fiber ultrafiltration of biologically treated wastewater. Cui and co-workers (Taha and Cui 2002, Taha *et al.* 2006) presented a CFD based modeling for a slug flow induced ultrafiltration in a tubular module. The calculation agreed well with the experimental data.

It is to be mentioned that all the above works mainly include gas sparged ultrafiltration in slug and bubbly flow regime. No work has been reported in the stratified flow regime. The present work undertakes gas sparged ultrafiltration in the stratified flow regime. The solute used is pectin, a well known gel forming agent. A theoretical model is proposed to calculate the permeate flux during gel controlling ultrafiltration. The validity of the model is also investigated.

## 2. Theory

Fig. 1 shows the geometry and the characteristic features of the two phase flow in stratified regime. The channel is divided into two regions. The bottom part consists of liquid phase and the top part is of gas phase. The interface dividing these two parts is assumed to be smooth and horizontal. On the membrane surface, a thin layer of pectin gel of constant thickness is formed. The mass transfer boundary layer is developed over the gel layer. In Fig. 1,  $H$  is the total height of the channel,  $h$  is the half-height,  $h_1$  is the height of the liquid gas interface,  $c_0$  is the concentration of pectin in the solution and  $c_g$  is its gel layer concentration.

### 2.1 Velocity field

In Fig. 1, it is assumed that the flow is occurring in a rectangular channel and the membrane is

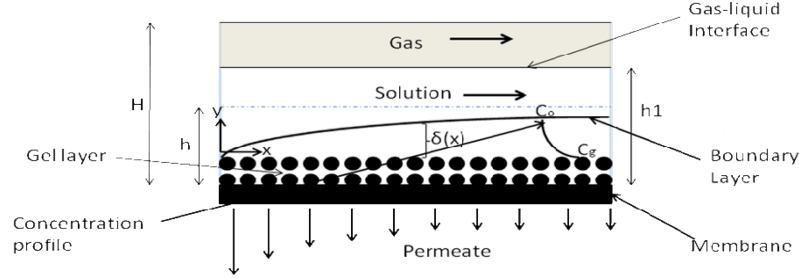


Fig. 1 Schematic of flow geometry

placed at the bottom. Since, the interest of analysis is solution of concentration field in the liquid layer, the velocity field is derived in that domain. Following assumptions are made:

(i) flow is steady; (ii) velocity field is laminar, fully developed, two dimensional and incompressible; (iii) Since the cross flow velocity is about 3 to 4 orders of magnitude higher than that of the permeation velocity, the effect of permeation is assumed to have negligible effects on x-axis velocity profile (De *et al.* 1997). Under these assumptions, the x-component equation of motion becomes

$$\frac{dp}{dx} = \mu \frac{d^2 u}{dy^2} \quad (1)$$

The relevant boundary conditions are

$$\text{at } y=0, u=0 \quad (2a)$$

$$\text{at } y=h_1, \frac{du}{dy}=0 \quad (2b)$$

The solution of Eq. (1) now becomes

$$u = \frac{1}{\mu} \left( \frac{dp}{dx} \right) \left[ h_1 y - \frac{y^2}{2} \right] \quad (3)$$

The volumetric flow rate of the liquid is defined as  $Q_L = u_0 h_1 w$ , where,  $u_0$  is the cross sectional average velocity in the liquid layer and  $w$  is the width of the channel. Thus, in terms of volumetric flow rate, integrating Eq. (3) over the height  $h_1$ , the expression of  $h_1$  is obtained as

$$h_1^3 = \frac{3\mu Q_L}{w \left( -\left( \frac{dp}{dx} \right) \right)} \quad (4)$$

The expression of average velocity,  $u_0$  is obtained as

$$u_0 = \frac{1}{3\mu} \left( -\frac{dP}{dx} \right) h_1^3 \quad (5)$$

Thus, the velocity profile in terms of average velocity in the liquid layer is

$$u = 3u_0 \left[ \frac{y}{h_1} - \frac{y^2}{2h_1^2} \right] \quad (6)$$

The average velocity in the liquid layer can be expressed in terms of superficial velocity of liquid in the channel as

$$u_0 h_1 = 2u_1 h \quad (7)$$

Where,  $h$  is the half channel height. Thus, the axial velocity profile in terms of superficial velocity of liquid in the channel becomes

$$u = 6u_1 \left( \frac{h}{h_1} \right) \left[ \frac{y}{h_1} - \frac{y^2}{2h_1^2} \right] \quad (8)$$

## 2.2 Concentration field

Pectin is a well known gel forming material (Rai *et al.* 2006). Thus, there is a formation of gel layer of constant gel concentration over the membrane surface as shown in Fig. 1. The gel layer concentration of pectin is  $38 \text{ kg/m}^3$  (Pritchard *et al.* 1995). Over the gel layer, mass transfer boundary layer grows slowly. Since the diffusivity of pectin is about  $4 \times 10^{-11} \text{ m}^2/\text{s}$  (Rai *et al.* 2007), Schmidt number for this solute is in the order of  $10^4$ . The thickness of mass transfer boundary layer is inversely proportional to Schmidt number ( $(\delta/h) \propto Sc^{-0.33}$ ) (Bird *et al.* 1960). Therefore, the thickness of mass transfer boundary layer is extremely small compared to the physical dimension (half height in this case) of the flow channel. Hence, within this thin, developing mass transfer boundary layer, the axial velocity profile can be approximated by neglecting  $y^2/h^2$  in Eq. (8). Therefore, the axial velocity profile within mass transfer boundary layer can be expressed as

$$u = 6u_1 \left( \frac{h}{h_1} \right) \left( \frac{y}{h_1} \right) \quad (9)$$

The governing equation for solute balance in mass transfer boundary layer is

$$u \frac{\partial c}{\partial x} + v \frac{\partial c}{\partial y} = D \frac{\partial^2 c}{\partial y^2} \quad (10)$$

Since, the thickness of mass transfer boundary layer is extremely small, it may be assumed that  $v \approx -v_w(x)$ , where,  $v_w$  is the permeation velocity at the wall.

In terms of non-dimensional variables, defined as,  $c^* = \frac{c}{c_0}$ ,  $x^* = \frac{x}{L}$ ,  $y^* = \frac{y}{h}$ , the governing equation of solute becomes

$$\frac{6u_1 h^2}{DL} \left( \frac{h}{h_1} \right)^2 y^* \frac{\partial c^*}{\partial x^*} - \frac{v_w h}{D} \frac{\partial c^*}{\partial y^*} = \frac{\partial^2 c^*}{\partial y^{*2}} \quad (11)$$

Defining, equivalent diameter of the channel as  $d_e = 4h$ , above equation can be cast as

$$Ay^* \frac{\partial c^*}{\partial x^*} - \frac{Pe_w}{4} \frac{\partial c^*}{\partial y^*} = \frac{\partial^2 c^*}{\partial y^{*2}} \quad (12)$$

where,  $A = \left( \frac{3}{8} Re.Sc. \frac{d_e}{L} \right) \cdot \left( \frac{h}{h_1} \right)^2$  and  $Pe_w = \frac{v_w d_e}{D}$ . The relevant boundary conditions for Eq. (10) are

$$\text{at } x = 0, c = c_0 \quad (13a)$$

$$\text{at } y = \delta, c = c_0 \quad (13b)$$

$$\text{at } y = 0, D \frac{\partial c}{\partial y} + v_w c_g = 0 \quad (13c)$$

In terms of non-dimensional variables, the boundary conditions become

$$\text{at } x^* = 0, c^* = 1 \quad (14a)$$

$$\text{at } y^* = \delta^*, c^* = 1 \quad (14b)$$

$$\text{at } y^* = 0, \frac{Pe_w}{4} c_g^* + \frac{\partial c^*}{\partial y^*} = 0 \quad (14c)$$

Eq. (12) is solved using integral method of analysis. In this method, the following concentration profile is assumed.

$$c^* = a_1 + a_2 \left( \frac{y^*}{\delta^*} \right) + a_3 \left( \frac{y^*}{\delta^*} \right)^2 \quad (15)$$

Eq. (15) satisfies the following conditions

$$\text{at } y^* = 0, c^* = c_g^* \quad (16a)$$

$$\text{at } y^* = \delta^*, c^* = 1 \quad (16b)$$

$$\text{at } y^* = \delta^*, \frac{\partial c^*}{\partial y^*} = 0 \quad (16c)$$

Using these boundary conditions, the concentration profile within mass transfer boundary layer now becomes

$$c^* = c_g^* - 2(c_g^* - 1) \left( \frac{y^*}{\delta^*} \right) + (c_g^* - 1) \left( \frac{y^*}{\delta^*} \right)^2 \quad (17)$$

The derivatives of  $c^*$  are presented below

$$\frac{\partial c^*}{\partial x^*} = 2(c_g^* - 1) \left[ \frac{y^*}{\delta^*} - \frac{y^{*2}}{\delta^{*3}} \right] \frac{\partial \delta^*}{\partial x^*} \quad (18a)$$

$$\frac{\partial c^*}{\partial y^*} = 2(c_g^* - 1) \left[ \frac{y^*}{\delta^{*2}} - \frac{1}{\delta^*} \right] \quad (18b)$$

$$\frac{\partial^2 c^*}{\partial y^{*2}} = 2(c_g^* - 1) \left[ \frac{1}{\delta^{*2}} \right] \quad (18c)$$

These derivatives are inserted in Eq. (12) and integrated across the boundary layer thickness.

$$\int_0^{\delta^*} \left[ A \frac{\partial \delta^*}{\partial x} \left( \frac{y^*}{\delta^*} - \frac{y^{*2}}{\delta^{*3}} \right) - \frac{Pe_w}{4} \left( \frac{y^*}{\delta^{*2}} - \frac{1}{\delta^*} \right) \right] dy^* = \int_0^{\delta^*} \left[ \left( \frac{1}{\delta^{*2}} \right) \right] dy^* \quad (19)$$

After integration and simplification, the governing equation of mass transfer boundary layer is obtained.

$$\frac{A \delta^* d\delta^*}{12 dx^*} + \frac{Pe_w}{8} = \frac{1}{\delta^*} \quad (20)$$

Putting value of  $\frac{\partial c^*}{\partial y^*}$  in Eq. (14c), the following expression is obtained.

$$Pe_w \delta^* = \frac{8(c_g^* - 1)}{c_g^*} \quad (21)$$

Combining Eqs. (20) and (21), the governing equation of  $\delta^*$  is obtained as

$$2A \delta^{*2} \frac{\partial \delta^*}{\partial x^*} - \frac{24}{c_g^*} = 0 \quad (22)$$

Integrating the above equation, an explicit expression of mass transfer boundary layer is now derived.

$$\delta^* = \left( \frac{36}{Ac_g^*} \right)^{1/3} x^{*1/3} \quad (23)$$

### 2.3 Mass transfer coefficient

The definition of mass transfer coefficient is

$$k(c_g - c_0) = -D \frac{\partial c}{\partial y} \Big|_{y=0} \quad (24)$$

In terms of non-dimensional variables, Eq. (24) becomes

$$Sh = k \frac{d_e}{D} = -\frac{4}{(c_g^* - 1)} \frac{\partial c^*}{\partial y^*} \Big|_{y^*=0} \quad (25)$$

Substituting  $\frac{\partial c^*}{\partial y^*}$  from Eq. (18b), and using the expression of thickness of mass transfer boundary layer, Eq. (23), the expression of Sherwood number becomes

$$Sh(x^*) = \frac{8}{\delta^*} = 8 \left( \frac{Ac_g^*}{36} \right)^{1/3} . x^{*-1/3} \quad (26)$$

The length averaged Sherwood number is

$$\overline{Sh} = \int_0^1 Sh(x) dx = 2.67 \left( Re.Sc. \frac{d_e}{L} \right)^{1/3} \cdot \left( \frac{h}{h_1} \right)^{2/3} . c_g^{*1/3} \quad (27)$$

#### 2.4 Length averaged permeate flux

From Eqs. (21) and (23), the profile of permeate flux is derived.

$$Pe_w(x^*) = \frac{8(c_g^* - 1)}{c_g^*} \left( \frac{A \cdot c_g^*}{36} \right)^{1/3} \cdot x^{*-1/3} \quad (28)$$

The length averaged permeate flux becomes

$$\overline{Pe_w} = \frac{12(c_g^* - 1)}{c_g^{*2/3}} \left( \frac{A}{36} \right)^{1/3} \quad (29)$$

Substituting the expression of  $A$ , the expression of dimensionless permeate flux is obtained.

$$\overline{Pe_w} = 2.67 \left( \text{Re} \cdot Sc \cdot \frac{d_e}{L} \right)^{1/3} \cdot \left( \frac{h}{h_1} \right)^{2/3} \cdot \frac{(c_g^* - 1)}{c_g^{*2/3}} \quad (30)$$

It may be noted that for  $\ln c_g^* \ll 3$ ,  $\frac{c_g^* - 1}{c_g^{*2/3}} = \ln c_g^*$  and at this limit, the average permeate flux becomes

$$\overline{Pe_w} = 2.67 \left( \text{Re} \cdot Sc \cdot \frac{d_e}{L} \right)^{1/3} \cdot \left( \frac{h}{h_1} \right)^{2/3} \cdot \ln c_g^* \quad (31)$$

#### 2.5 Pressure drop calculation for stratified flow

The friction factors for the laminar air flow through the rectangular channels were obtained by using the simplified (polynomial type) equation that fits the exact analytical solution within an accuracy of 0.05% (Hartnett and Kostic 1989, Lee and Lee 2001).

$$f \cdot \text{Re}_{d_e} = 24(1 - 1.3553\alpha + 1.9467\alpha^2 - 1.7012\alpha^3 + 0.9564\alpha^4 - 0.2537\alpha^5) \quad (32)$$

where,  $f$  is the friction factor and  $d_e$  is the equivalent diameter.  $\alpha$  denotes the aspect ratio defined as the value of the height divided by the width of the channel cross-section. The pressure drop expressions for only gas and only liquid phases (occupying the entire cross section) are presented below (Lee and Lee 2001).

$$\left( \frac{dp}{dx} \right)_{G0} = f_g \frac{\rho_g u_G^2}{d_e} \quad (33)$$

$$\left( \frac{dp}{dx} \right)_{L0} = f_l \frac{\rho_l u_l^2}{d_e} \quad (34)$$

Values of  $f_g$  and  $f_l$  are calculated using Eq. (32). In this study, the model derived by Wilkes is adopted to evaluate the pressure gradient in the filter channel (Wilkes 2006). According to this model, the pressure gradient of a liquid–gas two-phase flow  $(dp/dx)_{TP}$ , can be calculated by

$$\left( \frac{dp}{dx} \right)_{TP} = \phi_g^2 \left( \frac{dp}{dx} \right)_{G0} = \phi_l^2 \left( \frac{dp}{dx} \right)_{L0} \quad (35)$$

where,  $\phi_g$  and  $\phi_l$  are the multipliers. The value of  $\left(\frac{dp}{dx}\right)_{G0}$  or  $\left(\frac{dp}{dx}\right)_{L0}$  are related through the parameter  $X$  as

$$X^2 = \frac{\left(\frac{dp}{dx}\right)_{L0}}{\left(\frac{dp}{dx}\right)_{G0}} = \frac{\phi_g^2}{\phi_l^2} \quad (36)$$

$X$  is known as Martinelli's parameter. Classical Lockhart Martinelli (Lockhart and Martinelli 1949) type correlation is

$$\phi_l^2 = 1 + \frac{c}{X} + \frac{1}{X^2} \quad (37)$$

Mishima and Hibiki (1996) has proposed a correlation for parameter  $C$  as a function of the equivalent diameter as follows

$$c = 21[1 - \exp(-0.319d_e)] \quad (38)$$

Knowing the system geometry, the friction factors for gas and liquid phases are calculated from Eq. (32). With the knowledge of gas and liquid flow rates, the pressure drop of gas only and liquid only phases can be calculated from Eqs. (33) and (34). Now, calculating  $X$  from Eq. (36) and  $c$  from Eq. (38),  $\phi_l^2$  is calculated.  $\phi_g^2$  can be calculated from Eq. (36) and two phase pressure drop can be estimated from Eq. (35). With the estimation of pressure drop, gas-liquid interface height,  $h_1$ , can be calculated from Eq. (4). After that, using Eqs. (28) and (31) length averaged Sherwood number and dimensionless permeate flux can be estimated.

### 3. Experimental

#### 3.1 Materials

An organic thin film composite membrane of molecular weight cut off 30 kDa, consisting of a polyamide skin over a polysulphone support was used for ultrafiltration. The membrane was purchased from M/s, Permionics India Pvt. Ltd., Baroda, Gujarat, India. Pectin (molecular weight 30000-100000, degree of esterification 63-66%) supplied by M/s, Loba-Chemie, Mumbai, India was used as the model solute. Nitrogen gas was used for gas sparging.

#### 3.2 Membrane set up assembly

A rectangular cross flow cell, made of stainless steel, was designed and fabricated. The cell consisted of two matching flanges as shown in Fig. 2(a). The inner surface of the top flange is mirror polished. The bottom flange is grooved, forming the channels for the permeate flow. The channels in the bottom flange with the internal grid structure are shown in Fig. 2(b). A porous stainless steel plate is placed on the lower flange that provides mechanical support to the membrane.

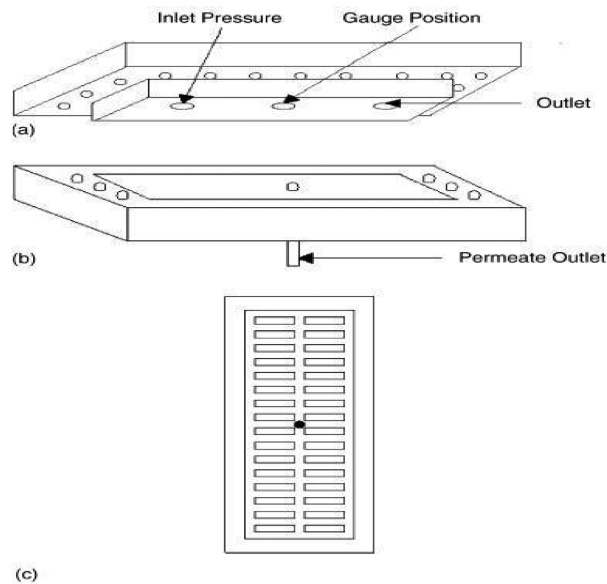


Fig. 2 Membrane module assembly. ; (a) Top flange; (b) bottom flange; (c) top view of bottom flange

Two neoprene rubber gaskets are placed over the membrane; the top view of which is shown in Fig. 2(c). The effective length, width and height of the membrane channel were 14.6 cm, 5.5. cm and 3.4 mm.

### 3.3 Membrane cell with air sparging set-up

For experiments with gas sparging, nitrogen was injected from a pressurized cylinder through a gas rotameter to the membrane cell along with the feed. The gas flow rate was controlled by a stainless steel regulator attached to the outlet of the cylinder. Two non-return valves prevent backflow of gas. The feed (pectin solution) was pumped by a high pressure reciprocating pump from the stainless steel feed tank to the cross flow cell with a rectangular channel. The retentate stream was recycled to the feed tank. The liquid flow rate was measured by a rotameter in the retentate line and the pressure inside the membrane cell was controlled by a bypass valve. The pressure and the cross flow rate inside the membrane channel were independently set by operating the valves in the bypass line and that at the outlet of the membrane cell. Permeate samples were collected from the bottom of the cell to measure the permeate flux and concentration. The schematic of the experimental set up is shown in Fig. 3.

### 3.4 Experimental design

Ultrafiltration experiments with pectin were designed to observe the effects of variation in operating conditions such as liquid and gas flow rate. The transmembrane pressure drop was fixed at 276 kPa. A pectin solution of concentration  $1 \text{ kg/m}^3$  was used for all the experiments. The viscosity of this solution was measured by Ostwald viscometer and it was  $1.75 \times 10^{-3} \text{ Pa.s}$ . The gas flow rates were varied in the range of 5 to 40 l/h. The liquid flow rate were varied in the range of 60 to 90 l/h.

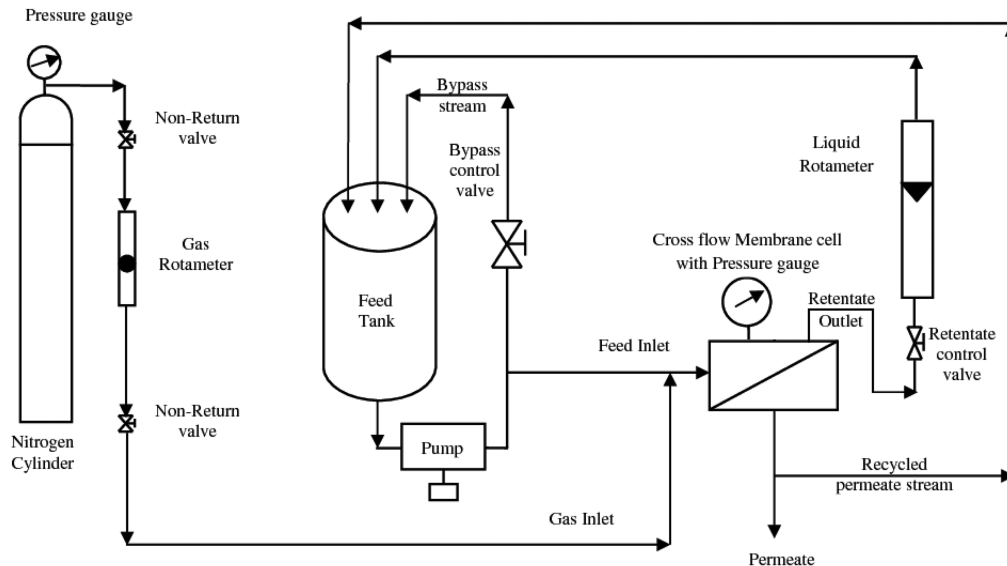


Fig. 3 Schematic of experimental set up

### 3.5 Experimental procedure

The steps used in the experiments are as follows:

1. *Compaction of membranes*: Fresh membrane was compacted at a pressure of 414 kPa for 2.5 hour using distilled water.
2. *Permeability measurement*: After compaction, ultrafiltration experiments were conducted at various trans-membrane pressure drops using distilled water. The membrane permeability was estimated from the slope of permeate flux versus pressure drop plot. The permeability of the membrane was found to be  $1 \times 10^{10}$  m/(Pa·s). Permeability values varied within  $\pm 3\%$  between the experiments.
3. *Conduction of the experiment*: The feed was kept in a stainless steel feed tank of 2 liter capacity. For conducting gas sparging experiments, nitrogen gas and feed solution were simultaneously injected to the membrane cell with their respective flow rates according to the experimental design. Nitrogen was introduced first into the membrane cell from a pressurized cylinder through a gas rotameter. A high pressure reciprocating pump was used to pump the feed into the cross flow membrane cell. Cumulative volumes of permeate were collected during the experiment. The permeate stream was recycled to maintain a constant concentration in the feed tank. Permeate samples were collected at different time intervals for analysis. A bypass line was provided from the pump delivery to the feed tank. Retentate and bypass control valves were used to vary the pressure and flow rate independently. Values of permeate flux were determined from the slopes of cumulative volume versus time plot. The precision of flux measurement was  $\pm 5\%$ . Permeate samples were analyzed.

### 3.6 Analysis

The permeate samples were analyzed using a spectrophotometer at a wavelength of 280 nm using

a UV-Visible Spectrophotometer (Perkin Elmer, Connecticut, USA).

## 4. Results and discussion

### 4.1 Variation of gas-liquid interface with liquid and gas flow rate

As described in section 3.4, gas flow rate varies from 5 to 40 l/h and liquid flow rate is in the range of 60 to 90 l/h. The mass flux of liquid and gas in the flow channel are in the range of 89 to 133 kg/m<sup>2</sup>.s and 0.01 to 0.073 kg/m<sup>2</sup>.s respectively. From a classical flow regime map (Brennen 2005), it may be identified that with these set of operating conditions, the flow regime belongs to stratified region. As outlined at the end of section 2, the height of gas-liquid interface can be calculated, for a set of operating conditions (gas and liquid flow rate). Variation of height of gas-liquid interface with gas flow rate for different liquid flow rates is presented in Fig. 4. It is observed from this figure that the height of gas-liquid interface decreases with gas flow rate. At a fixed liquid flow rate, with increase in gas flow rate, forced convection increases resulting in an enhancement of shear at the interface. This leads to a decrease in the interface height. As gas flow rate increases from 0 to 40 l/h, the interface height decreases from 3.4 to 1.83 mm for liquid flow rate 60 l/h (Re=606). For liquid flow rate 90 l/h (Re=909), interface height decreases from 3.4 to 1.92 mm in the same range of gas flow rate. At a fixed gas flow rate, the interface height increases with liquid flow rate. With increase in liquid flow rate, more liquid is accommodated, leading to pushing up the height of interface. At gas flow rate of 40 l/h, the interface height increases from 1.83 to 1.92 mm as the liquid flow rate increases from 60 to 90 l/h.

### 4.2 Variation of boundary layer thickness and mass transfer coefficient with liquid and gas flow rate

With calculation of height of gas-liquid interface, as a function of gas and liquid flow rates, Eq. (23)

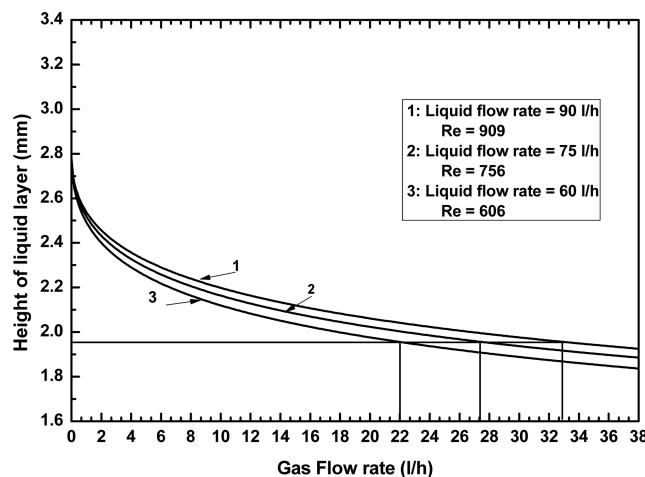


Fig. 4 Variation of height of gas-liquid interface with the gas flow rate at various liquid flow rates

is used to evaluate the thickness of mass transfer boundary layer for different gas and liquid flow rates. Profiles of mass transfer boundary layer thickness with the liquid and gas flow rates are shown in Fig. 5. In general, it can be observed from this figure that for all the operating conditions, the mass transfer boundary layer is developing over the channel length. The maximum thickness of boundary layer is two orders of magnitude less than the channel height. Curves 1 to 3 present the variation of boundary layer thickness for three values of gas flow rates at a fixed value of liquid flow rate of 60 l/h ( $Re=606$ ). As the gas flow rate increases from 0 to 20 l/h, the boundary layer thickness decreases. This is due to increase in shear for enhanced gas flow rate as discussed earlier. This will affect the thickness of the mass transfer boundary layer. Curves 3 to 5 present variation of liquid flow rate on the thickness of mass transfer boundary layer at a fixed gas flow rate at 20 l/h. Increase in liquid flow rate has two implications. First, it will affect the height of gas-liquid interface as shown in Fig. 4 and second, it will induce a shearing action on the mass transfer boundary layer by forced convection. These two have opposing effects. As shown in Fig. 4, with increase in liquid flow rate, the interface height increases, resulting in an enhancement of thickness of mass transfer boundary layer as it is inversely proportional to interface height (Eq. 27). But, increase in liquid flow rate increases the shear on the mass transfer boundary layer, thereby restricting its growth. Since the liquid layer is directly in touch with mass transfer boundary layer, this effect will be dominant and as a result, the thickness of mass transfer boundary layer decreases with the liquid flow rate as shown in this figure. Thickness of mass transfer boundary layer has direct implication on the resistance offered against the solvent flux through the membrane and it is reflected in mass transfer coefficient. Lower values of mass transfer boundary layer thickness, indicates higher mass transfer coefficient and improved system performance in terms of throughput (permeate flux) of the process. This is shown in Fig. 6. Variation of mass transfer coefficient with liquid and gas flow rates is presented in this figure. This figure clearly shows that the mass transfer coefficient increases with both gas and liquid flow rates. As discussed in Fig. 4, the boundary layer thickness decreases with both gas and liquid flow rates. These would result into proportional increase in mass transfer coefficient. At liquid flow rate, 60 l/h, the mass transfer coefficient increases from  $3.9 \times 10^{-5}$  to  $4.8 \times 10^{-5}$  m/s corresponding to increase in gas flow rate from 0 to 20 l/h. This amounts to an enhancement of mass transfer coefficient by 23%. For 75 and 90 l/h of liquid flow rates, the

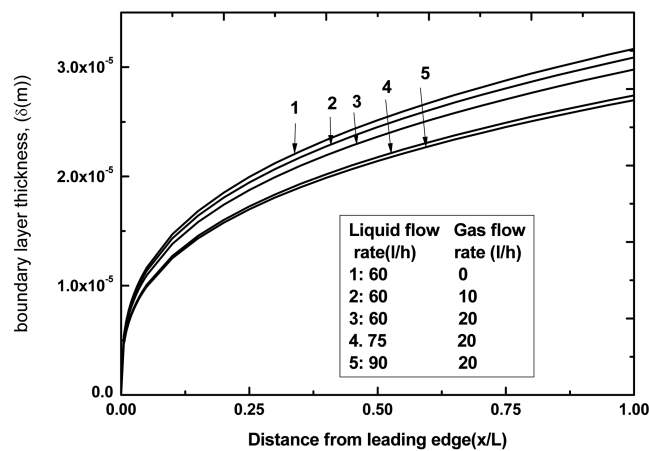


Fig. 5 Profile of mass transfer boundary layer thickness with the operating flow rates

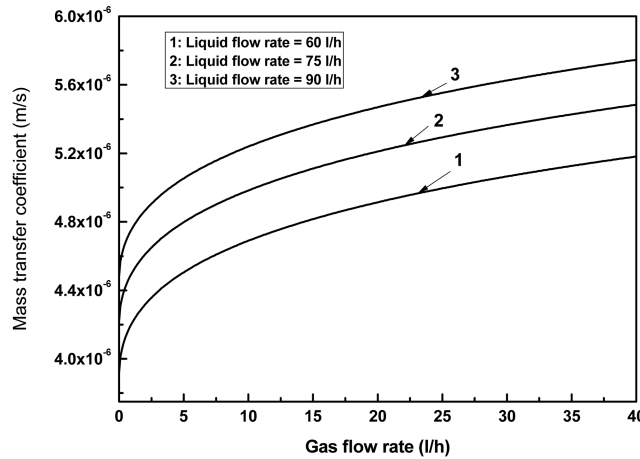


Fig. 6 Variation of mass transfer coefficient with the gas flow rate at various liquid flow rates

corresponding increase in mass transfer coefficient is 21% and 22%, respectively. For a fixed gas flow rate, the mass transfer coefficient increases with liquid flow rates. For gas flow rate at 10 l/h, the mass transfer coefficient increases from  $4.6 \times 10^{-5}$  to  $5.2 \times 10^{-5}$  m/s, i.e., an increase of about 13% for increase in liquid flow rate from 60 to 90 l/h. At 20 l/h of gas flow rate, the increase in mass transfer coefficient in the same range of liquid flow rate is about 13%. Thus, from this analysis it is clear that there is a distinct advantage of using a two phase stratified flow in a membrane channel and augmentation of mass transfer coefficient is significant.

#### 4.3 Variation of permeate flux profile with liquid and gas flow rate

Profiles of non-dimensional local permeate flux as function of operating condition are shown in Fig. 7. It is observed from this figure that non-dimensional permeate flux decreases along the module length. The decrease is sharp at the entrance of the channel and it is gradual in the channel

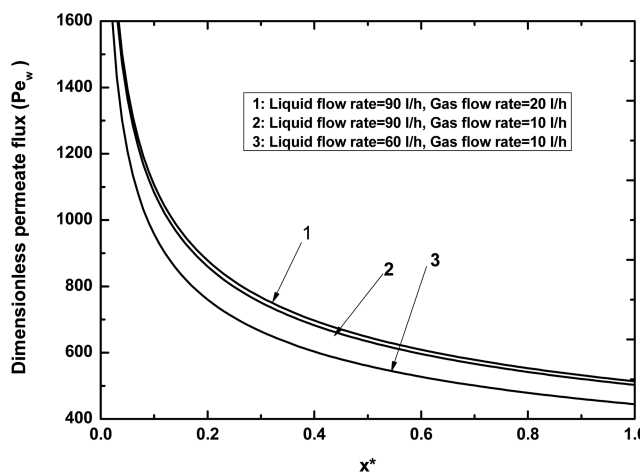


Fig. 7 Profile of mass transfer boundary layer thickness with the operating flow rates

downstream. As discussed earlier, the thickness of mass transfer boundary layer dictates the resistance against the solvent flux (permeate). Permeate flux is higher for a lower thickness of mass transfer boundary layer. Since at the entrance of the channel, boundary layer thickness is small, it results into a higher permeate flux. In the downstream of the channel, boundary layer thickness increases gradually leading to moderate decrease in non-dimensional permeate flux. Curves 1 and 2 of this figure, indicate the effect of gas flow rate on permeate flux. The permeate flux increases with gas flow rates at a fixed liquid flow rate and it increases with liquid flow rate at fixed gas flow rate (curves 2 and 3). As discussed earlier, with increase in gas and liquid flow rate, the mass transfer coefficient in the channel increases, leading to an increase in permeate flux.

#### 4.4 Comparison with experimental data and validation of theory

Knowing the gas and liquid flow rates one can estimate the gas-liquid interface height as described earlier. Using the estimated value of height of the interface, the length averaged permeate flux can be calculated using Eq. (31). For various sets of operating conditions, the permeate flux was calculated and the predictions are presented in Fig. 8. Comparison of the calculated values of average permeate flux with the experimental data is also shown in the same figure. It can be observed from this figure that the matching between calculated and experimental data are remarkably close (within  $\pm 3\%$ ) for all the gas flow rates and liquid flow rate of 90 l/h. For liquid flow rates of 60 and 75 l/h, the calculated values are matching closely with the experimental data upto a gas flow rate of 20 l/h. Beyond 20 l/h, the experimental data corresponding to 60 and 75 l/h show a mismatch with the calculated values. For these cases, the experiments were repeated three times and consistent results were obtained. At these operating conditions, the calculated values show an overprediction in the range of 23% to 38%. These observations need some discussion. It has been shown that the classical flow regimes in a gas-liquid system are valid for a channel height more than 2mm (Wambugans 1991). For a mini-channel (channel height  $< 2$  mm), bubbly region occurs at lower gas and liquid superficial velocity compared to macro-channels (Channel height  $\geq 2$  mm). As shown in

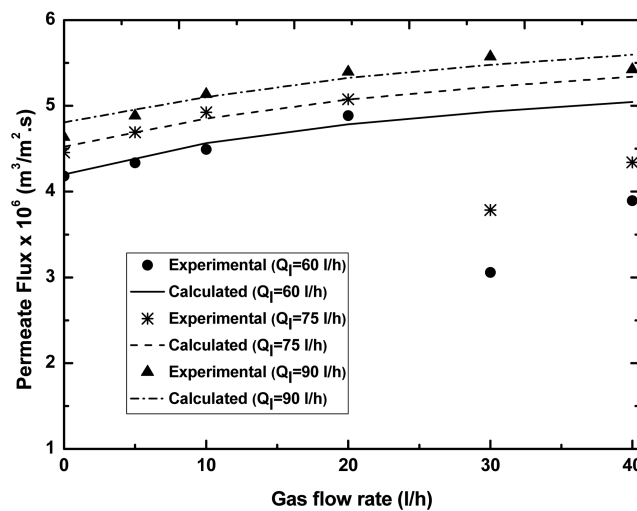


Fig. 8 Comparison of experimental and calculated permeate flux with operating conditions

Fig. 4, it can be observed that the height of gas-liquid interface becomes less than 2 mm for a gas flow rate of about 22, 27, 32 l/h corresponding to liquid flow rates of 60, 75 and 90 l/h, respectively. Therefore, beyond 20 l/h of gas flow rate for 60 and 75 l/h liquid flow rates, the flow regime converts from stratified to bubbly regime. As shown in Fig. 4, these effects are dominant for 60 and 75 l/h liquid flow rates and marginal for 90 l/h. In bubbly regimes, since bubbles are occurring in the bulk of the flow, they block some of the membrane surface and also dry patches appear thereby reducing the effective filtration area (Kabov 2007). These observations were also reported by other investigators (Abdel-Ghani 2000). Therefore, the theory proposed in this work for stratified flow regime fails to hold in the bubbly region for a mini-channel beyond 20 l/h of gas flow rate for liquid flow rates 75 and 90 l/h.

The flux enhancement due to two phase flow is also observed from this figure. At 90 l/h, the permeate flux increases to  $4.8 \times 10^{-6}$  to  $5.5 \times 10^{-6}$  m<sup>3</sup>/m<sup>2</sup>.s (14.6% increase) when the gas flow rate increases from 0 to 40 l/h. For 75 l/h of liquid flow rate, flux enhancement is 14% and for 60 l/h, this enhancement is 17% up to gas flow rate of 20 l/h.

## 5. Conclusions

Use of gas sparging under the stratified flow regime to the gel layer controlling ultrafiltration in a horizontal rectangular channel has been investigated in this paper. A flux enhancement of up to 14 to 17% has been observed in the range of the operating conditions studied herein. A mass transfer model for two phase gel layer controlling ultrafiltration has been developed for the stratified flow regime from first principles under the framework of boundary layer analysis. The model analysis shows that the flux enhancement is due to the enhancement mass transfer coefficient with gas flow rates. It is observed that for the liquid flow rates of 60 and 75 l/h, the permeate flux decreases beyond the gas flow rate of 20 l/h. This has been identified due to the change in flow regime to bubbly flow under those operating conditions and appearance of dry patches over the membrane surface. Thus, in this study, it has been identified that the gas flow rate can be upto 20 l/h to have a significant enhancement of flux during stratified two phase regime in an ultrafiltration system.

## References

- Abdel-Ghani, M.S. (2000), "Cross flow ultrafiltration of an aqueous polymer foam solution produced by gas sparging", *J. Membrane Sci.*, **171**, 105-117.
- Belfort, G., Mikulasek, P., Pimbley, J.M. and Chung, K.Y. (1993), "Diagnosis of membrane fouling using a rotating annular filter. 2. Dilute particle suspensions of known particle size", *J. Membrane Sci.*, **77**, 23-39.
- Bellara, S.R., Cui, Z.F. and Pepper, D.S. (1997), "Fractionation of BSA and lysozyme using gas sparged ultrafiltration in hollow fiber membrane module", *Biotechnol. Prog.*, **13**, 869-872.
- Bird, R.B., Stewart, W.E. and Lightfoot, E.N. (1960), *Transport Phenomena*, Wiley, New York, USA.
- Brennen, C.E. (2005), *Fundamentals of Multiphase Flow*, Cambridge University Press, London, UK.
- Cabassud, C., Laborie, S. and Laine, J.M. (1997), "How slug-flow can improve ultrafiltration flux in organic hollow fibers", *J. Membrane Sci.*, **128**, 93-101.
- Cheng, T.W., Yeh, H.M. and Wu, J.H. (1999), "Effects of gas slugs and inclination angle on the ultrafiltration flux in tubular membrane module", *J. Membrane Sci.*, **158**, 223-234.
- Cheng, T.W. (2002), "Influence of inclination on gas-sparged crossflow ultrafiltration through an inorganic tubular membrane", *J. Membrane Sci.*, **196**, 103-110.

- Chung, K.Y., Bates, R. and Belfort, G. (1993), "Dean vortices with wall flux in a curved channel membrane system: 4. Effect of vortices on permeation fluxes of suspensions in microporous membrane", *J. Membrane Sci.*, **81**, 139-150.
- Cui, Z.F. and Wright, K.L.T. (1994), "Gas-liquid two-phase crossflow ultrafiltration of dextrans and BSA solution", *J. Membrane Sci.*, **90**, 183-189.
- Cui, Z.F. and Wright, K.L.T. (1996), "Flux enhancement with gas sparging in downwards crossflow ultrafiltration: performance and mechanism", *J. Membrane Sci.*, **117**, 109-116.
- Cui, Z.F., Chang, S. and Fane, A.G. (2003), "The use of gas bubbling to enhance membrane processes", *J. Membrane Sci.*, **221**, 1-35.
- DaCosta, A.R., Fane, A.G. and Wiley, D.E. (1993), "Ultrafiltration of whey protein solutions in spacer filled flat channels", *J. Membrane Sci.*, **76**, 245-254.
- De, S., Bhattacharjee, S., Bhattacharya, P.K. and Sharma, A. (1997), "Generalized integral and similarity solution of the concentration profile for osmotic pressure controlled ultrafiltration", *J. Membrane Sci.*, **130**, 99-121.
- Delgado, S., X Díaz, V., Vera, L., Díaz, R. and Elmaleh, S. (2004), "Modelling hollow-fibre ultrafiltration of biologically treated wastewater with and without gas sparging", *J. Membrane Sci.*, **228**, 55-63.
- Ducom, G., Matamoros, H. and Cabassud, C. (2002), "Air sparging for flux enhancement in Nan filtration membranes: application to O/W stabilized and non-stabilised emulsions", *J. Membrane Sci.*, **204**, 221-236.
- Ducom, G., Puech, F.P. and Cabassud, C. (2002), "Air sparging with flat sheet nanofiltration: a link between wall shear stresses and flux enhancement", *Desalination*, **145**, 97-102.
- Fane, A.G., Fell, C.J.D. and Kim, K.J. (1985), "The effect of surfactant pretreatment on ultrafiltration of proteins", *Desalination*, **53**, 37-55.
- Finnigan, S.M. and Howell, J.A. (1990), "The effect of pulsed flow on ultrafiltration fluxes in a baffled tubular membrane system", *Desalination*, **79**, 181-202.
- Ghosh, R. and Cui, Z.F. (1999), "Mass transfer in gas sparged ultrafiltration: upward slug-flow in tubular membranes", *J. Membrane Sci.*, **162**, 91-103.
- Ghosh, R. (2006), "Enhancement of membrane permeability by gas sparging in submerged hollow fiber ultrafiltration of macromolecular solutions: Role of module design", *J. Membrane Sci.*, **274**, 73-82.
- Hartnett, J.P. and Kostic, M. (1989), "Heat transfer to Newtonian and non-Newtonian fluids in rectangular ducts", *Adv. Heat Transfer*, **19**, 247-356.
- Hermann, C.C. (1982), "High frequency excitation and vibration studies on hyperfiltration membranes", *Desalination*, **42**, 329-338.
- Imasaka, T., Kanekuni, N., So, H. and Yoshini, S. (1989), "Crossflow filtration of membrane fermentation broth by ceramic membranes", *J. Ferment. Bioeng.*, **68**, 200-206.
- Imasaka, T., So, H., Matsushita, K., Kurukawa, T. and Kanekuni, N. (1993), "Application of gas-liquid two-phase crossflow filtration to pilot-scale methane fermentation", *Drying Technol.*, **11**, 769-785.
- Kabov, O.A., Chinnov, E.A. and Cheverda, V.V. (2007), "Two-Phase Flow in Short Rectangular Mini-Channel", *Microgravity Sci. Technol.*, XIX-3/4, 44-47.
- Kramer, P.W., Yeh, Y.S. and Yasuda, H. (1989), "Low temperature plasma for the preparation of separation membranes", *J. Membrane Sci.*, **46**, 1-28.
- Lee, C., Chang, W. and Ju, Y. (1993), "Air slugs entrapped cross flow filtration of bacteria suspension", *Biotechnol. Bioeng.*, **41**, 525-530.
- Lee, H.J. and Lee, S.Y. (2001), "Pressure drop correlations for two-phase flow within horizontal rectangular channels with small heights", *Int. J. Multiphase Flow*, **27** (5), 783-796.
- Li, Q.Y., Cui, Z.F. and Pepper, D.S. (1997), "Fractionation of HSA and IgG by gas sparged ultrafiltration", *J. Membrane Sci.*, **136**, 181-190.
- Li, Q.Y., Cui, Z.F. and Pepper, D.S. (1997), "Effect of bubble size and frequency on the permeate flux of gas sparged ultrafiltration with tubular membranes", *Chem. Eng. J.*, **67**, 71-75.
- Li, Q.Y., Cui, Z.F. and Pepper, D.S. (1998), "Enhancement of ultrafiltration by gas sparging with flat sheet membrane modules", *Sep. Purif. Technol.*, **14**, 79-83.
- Llanos, J., Pérez, Á. and Cañizares, P. (2009), "Water-soluble polymer ultrafiltration process at pilot scale: Study of hydrodynamics and factors limiting flux", *J. Membrane Sci.*, **341**, 37-45.
- Lockhart, R.W. and Martinelli, R.C. (1949), "Proposed correlation of data for isothermal two-phase, two-

- component flow in pipes”, *Chem. Eng. Progr.*, **45**(1), 39-48.
- Mackley, M.R. and Sherman, N.E. (1993), “Cake filtration mechanisms in steady and unsteady flows”, *J. Membrane Sci.*, **77**, 113-121.
- Mercier, M., Fonade, C. and Lafforgue-Delorme, C. (1997), “How slug flow can enhance the ultrafiltration flux in mineral tubular membranes”, *J. Membrane Sci.*, **128**, 103-111.
- Mercier, M., Maranges, C., Lafforgue, C., Fonade, C. and Line, C. (2000), “Hydrodynamics of slug-flow applied to cross-flow filtration in narrow tubes”, *AIChE J.*, **46**, 476-488.
- Mishima, K. and Hibiki, T. (1996), “Some characteristics of air–water two-phase flow in small diameter vertical tubes”, *Int. J. Multiphase Flow*, **22**, 703-712.
- Mourouzidis-Mourouzis, S.A. and Karabelas A.J. (2008), “Whey protein fouling of large pore-size ceramic microfiltration membranes at small cross-flow velocity”, *J. Membrane Sci.*, **323**, 17-27.
- Najarian, S. and Bellhouse, B.J. (1996), “Effect of liquid pulsation on protein fractionation using ultrafiltration processes”, *J. Membrane Sci.*, **114**, 245-253.
- Nystrom, M. and Jarvinen, P. (1991), “Modification of polysulfone ultrafiltration membranes with UV irradiation and hydrophilicity increasing agents”, *J. Membrane Sci.*, **60**, 275-296.
- Porter, M.C. (2005), *Ultrafiltration*, in: M. C. Porter (Ed.) *Handbook of Industrial Membrane Technology*, Crest Publishing House, New Delhi, India, 2005.
- Pritchard, M., Howell, J.A. and Field, R.W. (1995), “The ultrafiltration of viscous fluids”, *J. Membrane Sci.*, **102**, 223-235.
- Rai, P., Majumdar, G.C., DasGupta, S. and De, S. (2006), “Modeling of Sucrose Permeation through a Pectin Gel during Ultrafiltration of Depectinized Mosambi (*Citrus sinensis* (L.) Osbeck) Juice”, *J. Food Sci.*, **71**(2), E87-94.
- Rai, P., Majumdar, G.C., DasGupta, S. and De, S. (2007), “Modeling of permeate flux decline of synthetic fruit juice and mosambi juice (*Citrus sinensis* (L.) Osbeck) in stirred continuous ultrafiltration”, *LWT Food Sci. Technol.*, **40**, 1765-1773.
- Rautenbach, R. and Albrecht, R. (1986), *Membrane Processes*, John Wiley, New York, USA.
- Rosenberg, E., Hepbildikler, S., Kuhne, W. and Winter, G. (2009), “Ultrafiltration concentration of monoclonal antibody solutions: Development of an optimized method minimizing aggregation”, *J. Membrane Sci.*, **342**, 50-59.
- Sarkar, B. and De, S. (2011), “Prediction of permeate flux of turbulent flow in cross flow electric field assisted ultrafiltration”, *J. Membrane Sci.*, **369**, 77-87.
- Steuck, M.J. and Reading, N. (1986), “Porous membranes having hydrophilic surface and processes”, *US Patent*, 4,618,533.
- Taha, T. and Cui, Z.F. (2002), “CFD modelling of gas-sparged ultrafiltration in tubular membranes”, *J. Membrane Sci.*, **210**, 13-27.
- Taha, T., Cheong, W.L., Field, R.W. and Cui, Z.F. (2006), “Gas-sparged ultrafiltration using horizontal and inclined tubular membranes—A CFD study”, *J. Membrane Sci.*, **279**, 487-494.
- Thomas, D.G. (1972), “Forced convection mass transfer in hyperfiltration at high fluxes”, *Ind. Eng. Chem. Fundam.*, **12**, 396-405.
- Wambuganss, M.W., Jendrzeczyk, J.A. and France, D.M. (1991), “Two-Phase flow patterns and transition in a small, horizontal, rectangular channel”, *Int. J. Multiphase flow*, **17**(3), 327-342.
- Wilkes, J.O. (2006), *Fluid Mechanics for Chemical Engineers*, Prentice Hall, New Jersey, USA.
- Wu, C., Zhang, S., Yang, D., Wei, J., Yan, C. and Jian, X. (2006), “Preparation, characterization and application in wastewater treatment of a novel thermal stable composite membrane”, *J. Membrane Sci.*, **279**, 238-245.
- Zhao, H., Price, W.E. and Wallace, G.G. (1993), “Transport of copper (II) across stand alone conducting polymer membranes”, *Polymer*, **34**, 16-20.

## Nomenclature

$c$	concentration ( $\text{kg/m}^3$ )
$c_0$	bulk concentration of Pectin ( $\text{kg/m}^3$ )
$c_g$	gel layer concentration ( $\text{kg/m}^3$ )
$c^*$	non-dimensional concentration ( $c/c_0$ )
$c_g^*$	non-dimensional gel layer concentration ( $c_g/c_0$ )
$D$	diffusivity of pectin ( $\text{m}^2/\text{s}$ )
$d_e$	equivalent diameter (m)
$f$	friction factor
$f_l$	only liquid friction factor
$f_g$	only gas friction factor
$H$	total height of the channel (m)
$h$	half-height of the channel (m)
$h_l$	height of liquid-gas interface (m)
$k$	Mass Transfer coefficient (m/s)
$L$	length of the membrane (m)
$\overline{Pe_w}$	Peclet number ( $v_w \cdot d_e/D$ )
$\overline{Pe_w}$	length averaged Peclet number
$p$	pressure ( $\text{N/m}^2$ )
$Q_L$	volumetric flow rate of liquid ( $\text{m}^3/\text{s}$ )
$Re$	Reynolds number
$Sc$	Schmidt number
$\overline{Sh}$	Sherwood number ( $k \cdot d_e/D$ )
$\overline{Sh}_L$	length averaged Sherwood number
$w$	width of the membrane (m)
$x$	distance from leading edge of the membrane (m)
$x^*$	non-dimensional distance from the leading edge of the membrane ( $x/L$ )
$y$	distance from top surface of the gel layer (m)
$y^*$	non-dimensional distance from top surface of the gel layer ( $y/h$ )
$u$	axial velocity (m/s)
$u_0$	cross sectional average velocity (m/s)
$u_l$	superficial liquid velocity (m/s)
$u_G$	gas only superficial gas velocity (m/s)
$u_L$	liquid only superficial liquid velocity (m/s)
$v$	transverse velocity (m/s)
$v_w$	liquid flux permeating through the membrane wall ( $\text{m}^3/\text{m}^2 \cdot \text{s}$ )
$(dp/dx)_{GO}$	gas only pressure gradient (pa/m)
$(dp/dx)_{LO}$	liquid only pressure gradient (pa/m)
$(dp/dx)_{TP}$	Total pressure gradient (pa/m)

### Greek Symbols

$\delta$	thickness of mass transfer boundary layer (m)
$\delta^*$	non-dimensional thickness of mass transfer boundary layer ( $\delta/h$ )
$\mu$	viscosity of the liquid (Pa.s)
$\rho_g$	gas density ( $\text{kg/m}^3$ )
$\rho_l$	liquid density ( $\text{kg/m}^3$ )